



Meteorology driving the highest ozone level occurred during mid-spring to early summer in Shanghai, China

Luyu Chang ^{a,d}, Fangfang He ^{a,d,*}, Xuexi Tie ^{b,c,d,**}, Jianming Xu ^{a,d}, Wei Gao ^{a,d}

^a Shanghai Climate Center, Shanghai Meteorological Service, Shanghai 200030, China

^b KLACP, SKLLQG, Institute of Earth Environment, Chinese Academy of Science, Xi'an 710061, China

^c Center for Excellence in Urban Atmospheric Environment, Institute of Urban Environment, Chinese Academy of Sciences, Xiamen 361021, China

^d Shanghai Key Laboratory of Meteorology and Health, Shanghai 200030, China



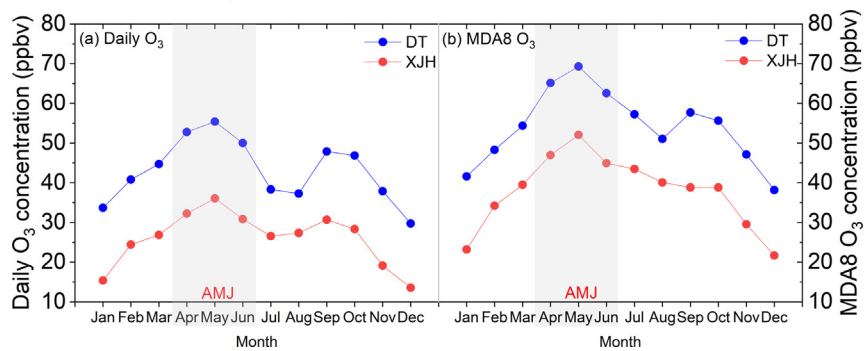
HIGHLIGHTS

- The maximum monthly O₃ level occurred during mid-Spring to early-Summer in Shanghai.
- The weather of G-SW is most favorable for high O₃ productions in Shanghai.
- The O₃ level in G-SW presents the most significant increasing trend from 2010 to 2019 in Shanghai.
- VOCs reduction significantly alleviates the peak O₃ concentration in G-SW in Shanghai.

GRAPHICAL ABSTRACT

We observed the most elevated mean daily and maximum daily 8-h (MDA8) O₃ concentrations occurred from mid-Spring to early Summer (AMJ) in Shanghai compared to other warm months, based on the long-term measurements from 2010 to 2019. The key weather pattern (G-SW) driving the greatest ozone production and accumulation in this period is recognized by the T-mode principal component approach (T-PCA). More importantly, the MDA8 O₃ concentration presents the greatest increasing rate from 2010 to 2019 in Shanghai downtown in the weather pattern of G-SW, suggesting that more occurrence and faster exacerbation of O₃ pollutions could be expected in the future. Process analysis by a chemical/dynamical model (WRF-Chem) is conducted to elucidate the strong O₃ productivity (19 ppbv/h in daytime), that dominates the high O₃ occurrence under the G-SW weather condition. Sensitive studies suggest that reduction of VOCs emissions is very effective to prevent the high O₃ pollution under G-SW in Shanghai, that photochemical productivity decreases by 35% in daytime response to 30% reduction of VOCs emissions, leading to 17.6% mitigation of peak O₃ concentration in Shanghai downtown. This result provides valuable information for the development of emission control strategy in Shanghai under different weather conditions.

Fig. 1 Monthly variations of (a) mean daily and (b) mean MDA8 O₃ concentrations observed at the urban site XJH and the rural site DT in Shanghai from 2010 to 2019. The shade rectangles denote the periods of Apr, and May and Jun, in which the O₃ presents higher levels than other months.



ARTICLE INFO

Article history:

Received 4 March 2021

Received in revised form 8 April 2021

Accepted 15 April 2021

Available online 22 April 2021

ABSTRACT

More recent studies highlighted the aggravated surface ozone (O₃) pollutions occurred in Spring and Autumn in China, but presenting clear distinctions for different cities. In this study, we observed the most elevated mean daily and maximum daily 8-h (MDA8) O₃ concentrations occurred from mid-Spring to early Summer (April, May and June, AMJ) at both urban and remote sites in Shanghai compared to other warm months (March, July,

* Correspondence to: F. He, Shanghai Climate Center, Shanghai Meteorological Service, Shanghai 200030, China.

** Correspondence to: X. Tie, KLACP, SKLLQG, Institute of Earth Environment, Chinese Academy of Science, Xi'an, 710061, China.

E-mail addresses: hff@soweaer.com (F. He), tiexx@iecas.ac (X. Tie).

Editor: Jianmin Chen

Keywords:
Weather classification
 O_3 pollution
WRF-Chem model
Shanghai

August, September, October), based on the long-term measurements from 2010 to 2019. The typical weather pattern of G-SW (High pressure with predominant winds of southwesterly) recognized by T-mode principal component approach (T-PCA), exhibits the strongest solar radiation and highest daily maximum temperature relative to other weathers in AMJ, leading to not only the most elevated O_3 concentration, but also the largest O_3 increasing variability in daytime. More importantly, under the G-SW weather condition, the MDA8 O_3 concentration presents the greatest increasing rate at 3.95 ppbv/yr from 2010 to 2019 in Shanghai downtown compared to other weather patterns, suggesting that more occurrence and faster exacerbation of O_3 pollutions could be expected under the G-SW weather condition in the future. To understand and mitigate high O_3 occurrences under the weather pattern of G-SW during AMJ, process analysis by a chemical/dynamical model (WRF-Chem, Weather Research and Forecasting (WRF) model coupled with Chemistry) is conducted to elucidate the strong O_3 productivity (19 ppbv/h in daytime), that dominates the high O_3 occurrence under the G-SW weather condition. Sensitive studies suggest that under the G-SW weather condition, reduction of VOCs emissions is very effective to prevent the high O_3 pollution in Shanghai. The model results show that photochemical productivity decreases by 35% in daytime response to 30% reduction of VOCs emissions, leading to 17.6% mitigation of peak O_3 concentration in Shanghai downtown. This result provides valuable information for the development of emission control strategy in Shanghai under different weather conditions.

© 2021 Published by Elsevier B.V.

1. Introduction

As an important atmospheric oxidant, ground ozone (O_3) is harmful to vegetation and human health (Yue and Unger, 2014; Feng et al., 2015; Goodman et al., 2015). It is also regarded as the third most important greenhouse gases, which accelerates the global warming (Sitch et al., 2007). Tropospheric O_3 is produced by photochemical reactions between nitrogen oxides (NOx) and volatile organic compounds (VOCs) in the presence of sunlight (Sillman, 2003). To date, China has experienced more and more severe ground O_3 pollutions in warm seasons (Lu et al., 2018), particularly in megacities such as Beijing and Shanghai, O_3 has become the primary air pollutant instead of fine particle in recent years. Thus, identifying drivers for the high O_3 occurrence in megacities needs to be deeply investigated in present and future studies.

In addition to the precursors of NOx and VOCs, meteorological conditions also play the important role in surface O_3 production and accumulation (Jacob and Winner, 2009; Dang et al., 2021). O_3 is directly formed by the combination reaction of atomic oxygen (O^3P) and molecular oxygen (O_2). In the troposphere, photolysis of NO_2 at wavelengths ≤ 424 nm is the primary source of O^3P atoms and prompts O_3 formation. As a result, the activity of O_3 production is substantially affected by UV radiation, which is largely determined by cloud cover and water vapor in the atmosphere. Gao et al. (2017) observed the sharp decline of O_3 occurred in June in Shanghai due to the Meiyu period with deep and persistent cloud cover impeding solar radiation to reach the surface of the Earth. Different from its precursors of NOx and VOCs with short chemical life, O_3 has the relative longer lifetime of about one month. It could be transported to downwind of several hundred kilometers by horizontal winds (Wang et al., 2006), leading to more regional air pollution issues. Hu et al. (2018) and Zheng et al. (2021) both reported the trans-boundary O_3 events from urban to meso-scale to aggravate local air quality over Yangtze River Delta (YRD) region by model studies. Recently, Gu et al. (2020a) observed much higher O_3 concentration at the offshore island than the urban center of Shanghai. The daily maximum O_3 concentration in the coastal city was deteriorated by 20–30% due to the onshore sea breeze carrying air mass of enhanced O_3 . It was summarized by Wang et al. (2017) that high O_3 episodes often occurred on clear weather condition with high temperature, little cloudiness, dry air and light winds to facilitate O_3 photochemical production and accumulation.

Since local weather conditions such as cloud cover, temperature and horizontal wind are greatly determined by atmospheric circulations, the chemical and physical processes of O_3 are noticeably sensitive to weather patterns. The synoptic and its evolutions are suggested to have great effects on the daily to monthly O_3 variations which have been reported by several studies, e.g., Asian continental high (Ding et al., 2013), western pacific subtropical high (WPSH, Shu et al., 2016;

Pu et al., 2017), typhoon (Zhang et al., 2013; Jiang et al., 2015), Eastern Asian westerly jet (Ding and Wang, 2006; Ni et al., 2018) etc. However, considerable uncertainties still exist among repercussions of the weather patterns on O_3 levels and its variations in different regions at different latitude, with distinctive topography and land cover. For example, located close to the center of summertime WPSH, the northern China often experiences sunny and dry weather, resulting in elevated surface O_3 concentrations (Wang et al., 2017). On the contrary, rich precipitation induced by damp southwesterly flows along southwest of the high in southern China significantly inhibits O_3 concentrations (Zhao and Wang, 2017). As such, weather patterns and their potential relationships with O_3 levels have to be carefully and separately conducted in diverse regions.

As the largest megacity in China, Shanghai has experienced elevated O_3 pollution due to considerable exhausts from anthropogenic activities in recent years (Geng et al., 2008; Tie et al., 2009; Gu et al., 2020a, b). Moreover, the O_3 concentration in Shanghai presented substantial increasing trends during the past 10 years as a result of emission reduction of NOx (Gao et al., 2017; Xu et al., 2019). In addition to the chemical regime of O_3 production in Shanghai which has been widely investigated by several studies (Geng et al., 2008; Tie et al., 2013), synoptic systems related to high O_3 occurrence have also been explored by Shu et al. (2020), Chang et al. (2019) and Gu et al. (2020b) etc. For example, strong solar radiation and high temperature related to WPSH, the significant subsidence flow from the typhoon peripherals, are all conducive to the occurrences of high O_3 episode in Shanghai. Such studies provided better understanding for the effects of synoptics on local O_3 pollutions, but mostly limited in hot summer (June, July and August). Several recent studies reported that O_3 pollution in spring and autumn exacerbated greatly than summer in Shanghai (Gu et al., 2020a), Beijing (Ma et al., 2016) and other cities, resulting in more and more elevated O_3 pollutions beyond summer. For example, the worst O_3 pollution event in 2019 taken place on May 23 in Shanghai, with daily maximum concentration reaching 163 ppbv. What driving such severe O_3 events beyond summer needs to be explored from wider viewpoints, including emissions, chemical regime, as well as meteorological conditions.

In this paper, long-term measurements of O_3 concentration from 2010 to 2019 in Shanghai are used to examine the monthly variations of the elevated O_3 levels. Then the predominant weather patterns during the period favorable for high O_3 occurrences are revealed based on the objective weather classification technique. In addition, the mechanism of O_3 production and accumulation under the specific weather patterns are investigated by comprehensive observations and model studies. Finally, the strategy to mitigate high O_3 pollution during the specific weather pattern is explored by model sensitive experiments. The long-term measurements of O_3 and meteorology, the reanalyzed

atmospheric circulations, as well as the weather classification method and WRF-Chem model are described in Section 2, the results and discussion of the subject are presented in Section 3, finally the main conclusions are showed in Section 4.

2. Data and method

2.1. Long-term O₃ measurements

Hourly measurements of O₃ concentration at an urban site (XJH) and a remote site (DT) in Shanghai from 2010 to 2019 are used in this study to investigate monthly and annual O₃ variabilities. As was documented by Xu et al. (2019), DT is located at a national natural reserve at a remote island with very few anthropogenic activities, observed O₃ well reflects the background of transport from Shanghai and its neighboring area. While XJH is located at the downtown of Shanghai with dense population and large transports, O₃ production is mostly driven by photochemical reactions of local emissions. We collect O₃ measurements at such two different sites, examines their variabilities, to elucidate the effects of specific weather patterns, while not emissions, on O₃ production and variation. The methodology, instrument and maintenance, as well as the quality control protocol for O₃ measurements, could be referred from Tie et al. (2013) and Gao et al. (2017). These data have been widely used to explore O₃ chemical regime, long term variation and its response to emission reduction in Shanghai (Gao et al., 2017; Xu et al., 2019; Gu et al., 2020a,b).

2.2. Meteorological data

The reanalysis data with 1° × 1° resolution from the European Centre for Medium-Range Weather Forecasts (ECMWF) for the fifth generation (ERA5, 2017) are used to aggregate weather patterns. Geopotential height, air temperature, wind speed of U and V at 925 hPa are extracted at 00:00, 06:00, 12:00 and 18:00 (BJT, local time used in the paper). To examine the key meteorological factors related to O₃ production under specific weather pattern, hourly meteorological measurements, including 2 m temperature (T2), relative humidity (RH), total solar radiation, precipitation, horizontal wind speed (WS) and direction at Shanghai Baoshan observatory are also collected during the same period. As the only national meteorological observatory in Shanghai, meteorological measurements at Baoshan are exchanged globally through the World Meteorological Organization (WMO), usually applied to describe the climatological characteristics in Shanghai.

2.3. Weather classification method

The obliquely rotated principal component analysis in the T-mode principal component approach (T-PCA) developed by Huth et al. (2008) in cost733class software package (<http://cost733.met.no/>) is used in this study to conduct atmospheric circulation classification related to O₃ pollution in Shanghai. The T-PCA method is less dependent on previous experiences, and more superior in dealing with large volumes of data (Huth, 1996), thus popularly used to investigate the specific weather pattern conducive to air pollutions in China (Xu et al., 2016; Miao et al., 2017; Liao et al., 2017). Instead of the single meteorological element used by T-PCA classification in previous studies, the daily average geopotential height combined with the wind-U and wind-V at 925 hPa are calculated simultaneously for weather classification in this study. According to the experience by Xu et al. (2016), the domain encompassing the region of 26°N–36°N, 114°E–124°E, were appropriate for the T-PCA method to obtain the major synoptic pattern affecting Shanghai.

2.4. WRF-Chem model configuration

In order to better understand the mechanism of O₃ production and accumulation in Shanghai under specific weather patterns, the WRF-Chem

model (version 3.9.1, <https://www2.acm.ucar.edu/wrf-chem>) (Grell et al., 2005) is applied for O₃ simulation under specific weather patterns. Process analysis technique in WRF-Chem is conducted to quantify the separate contributions of chemistry, advection and diffusion to local O₃ concentrations. The domain is set up with 6 km horizontal resolution, centered at 30.83°N, 119.3°E with 201 × 201 grids, and 30 vertical layers extending from the surface to 50 hPa. The Regional Acid Deposition Model, version 2 (RADM2) (Stockwell et al., 1990) is selected as the gas-phase chemical mechanism. Correspondingly, the Modal Aerosol Dynamics Model for Europe is chosen as the aerosol chemistry mechanism. Other parameterization schemes are referred from the work by Tie et al. (2013). The initial and boundary condition of meteorology is constrained by ERA5 reanalysis data, to be well consistent with the weather classification results. The boundary conditions of chemistry are constructed from a global chemical transport model (MOZART-4, Model for Ozone and Related chemical Tracers, version 4; Tie et al., 2001; Emmons et al., 2010). Anthropogenic emissions are provided by the Multi-resolution Emission Inventory for China (MEIC) (<http://www.meicmodel.org/>) for the year 2010 (Li et al., 2014), in which, NO_x, SO₂, CO and some VOC species were greatly improved over Shanghai by Tie et al. (2013) based on the MIRAGE-Shanghai campaign. The biogenic emissions are calculated online based on the Model of Emissions of Gas and Aerosols from Nature (MEGAN) (Guenther et al., 2006).

3. Results and discussions

3.1. Seasonal variations of O₃ concentrations in Shanghai

Fig. 1 presents the monthly variations of mean daily and maximum daily 8-h (MDA8) O₃ concentrations averaged between 2010 and 2019 at DT and XJH respectively. The O₃ level at XJH is much lower than that at DT in each month, which is consistent with the previous studies from Gao et al. (2017) and Gu et al. (2020a). For example, the MDA8 O₃ concentrations at XJH are observed as 46.2, 42.8, 35.7 and 26.4 ppbv in Spring, Summer, Autumn and Winter respectively, about 26–40% lower than those at DT. This is resulted from the VOCs-limited regime of O₃ chemical formation in Shanghai urban center (XJH), leading to substantial O₃ inhabitation due to large NO_x emissions (Xu et al., 2019). As showed in Fig. 1, observed O₃ at XJH and DT presents clear seasonal variations. Both daily and MDA8 O₃ concentrations climb quickly in spring and peak in May, while exhibit significant decline in hot summer (June–August). This is some different from the common features of seasonal variation of O₃ observed at typical mid-latitude cities (Wang et al., 2017), where the monthly O₃ level usually peaks in June or July. In Fig. 1, the top three maximums of both monthly mean O₃ concentration and monthly mean MDA8 O₃ concentration appear in May, April and June in sequence. That is to say, the period from mid-Spring to early Summer (April, May and June, referred as AMJ in the paper) takes over the highest O₃ concentrations in Shanghai. This is further highlighted in Fig. 2 that, the mean O₃ concentrations during AMJ are mostly higher than those in other warm months (Mar, June, August, September, October) from 2010 to 2019 at both DT and XJH sites. For example, the O₃ level in July exhibits clear drops of 14.4 and 6.5 ppbv at DT and XJH respectively relative to AMJ during 2010 to 2019. However, several O₃ anomalies are also observed in September with 3.1–7.7 ppbv higher than AMJ in 2015 and 2016, which need to be paid more attentions in future studies. It is noting that the highest O₃ level in AMJ is consistently observed at both urban site XJH and remote site DT, suggesting that it is not attributed to either local emissions or transports. Han et al. (2019) also reported the similar results that the monthly O₃ concentration peaked in late spring in other cities neighboring Shanghai, suggesting that it is not limited in Shanghai, but extends to a wider scale. Therefore, we speculate that the significantly higher O₃ concentration observed in AMJ in Shanghai is probably related to the specific weathers favorable for the O₃ production and accumulation, which has not been paid adequate attention in previous studies.

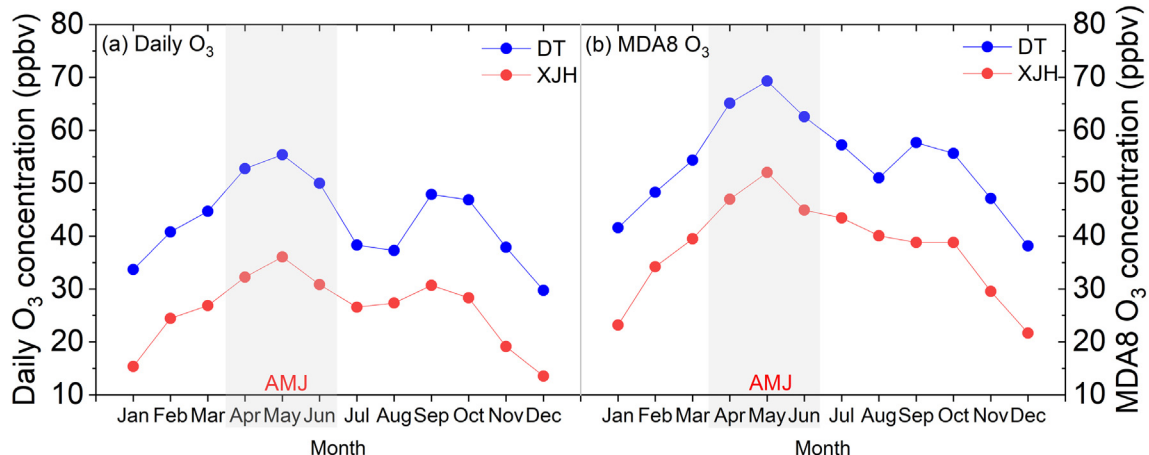


Fig. 1. Monthly variations of (a) mean daily and (b) mean MDA8 O₃ concentrations observed at the urban site XJH and the rural site DT in Shanghai from 2010 to 2019. The shade rectangles denote the periods of April, and May and June, in which the O₃ presents higher levels than other months.

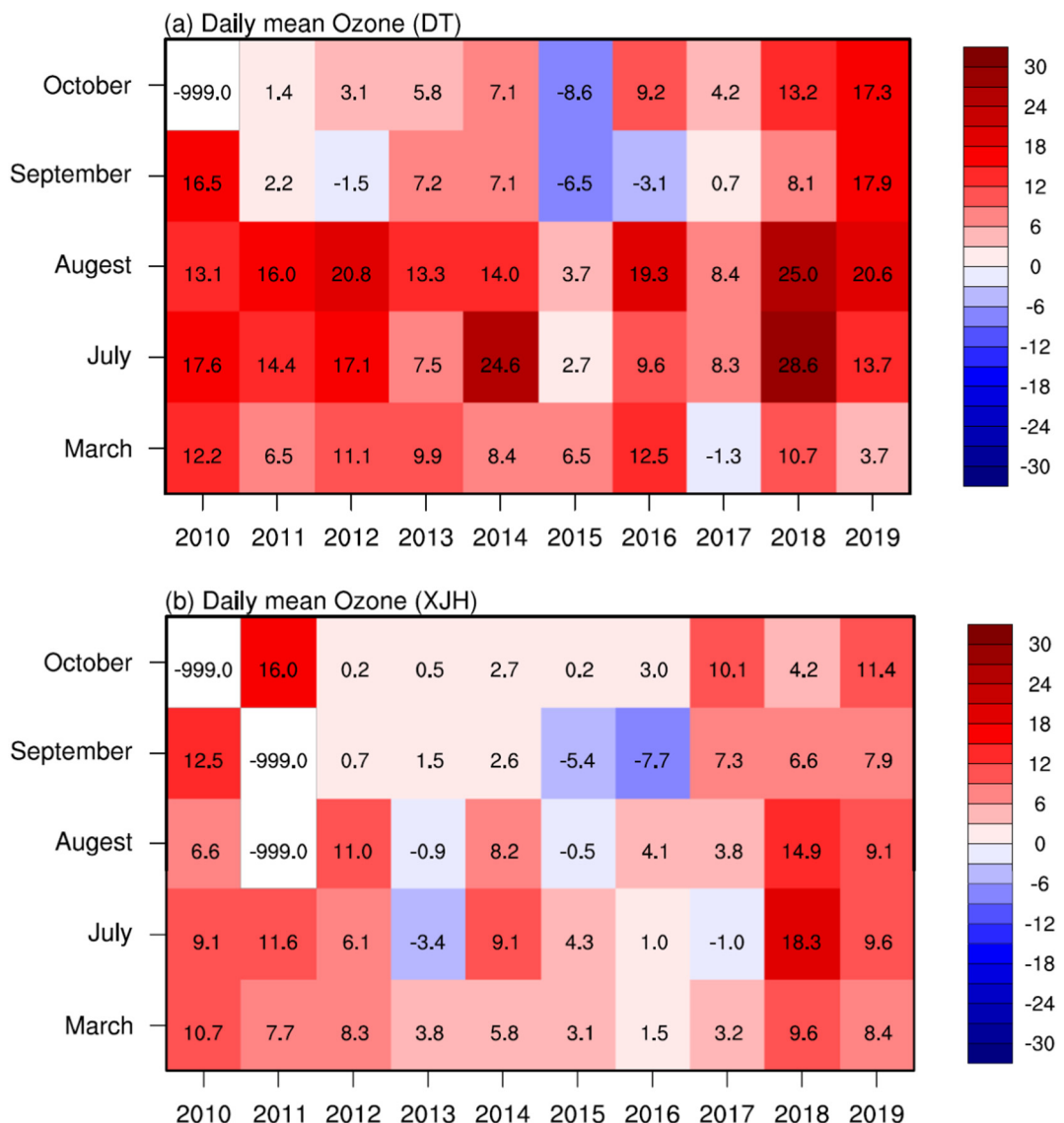


Fig. 2. The mean O₃ concentrations during AMJ minus the mean monthly O₃ concentration in each other warm month (March, July, August, September, October) from 2010 to 2019, at (a) XJH and (b) DT. The boxes filled with red color denote positive values (ppbv), indicating higher O₃ level during AMJ, while blues indicate lower O₃ level during AMJ. Whites denote missing measurements. (For interpretation of the references to color in this figure legend, the reader is referred to the web version of this article.)

3.2. Predominant weather patterns during AMJ

As described in Section 3.1, the highest monthly O₃ concentration in Shanghai is observed in AMJ, which is probably related to specific weather patterns. The meteorology favorable for O₃ production and accumulation in hot summer has been documented by previous studies,

that is closely connected to subtropical high. During late June to middle August, sunny and stagnant weather is expected in Shanghai under the control of subtropical high, leading to strong solar radiation and extremely high temperature, providing most favorable activities of photochemical reactions. However, during AMJ, the summer monsoon has not fully onset, the main part of subtropical high is still far away from

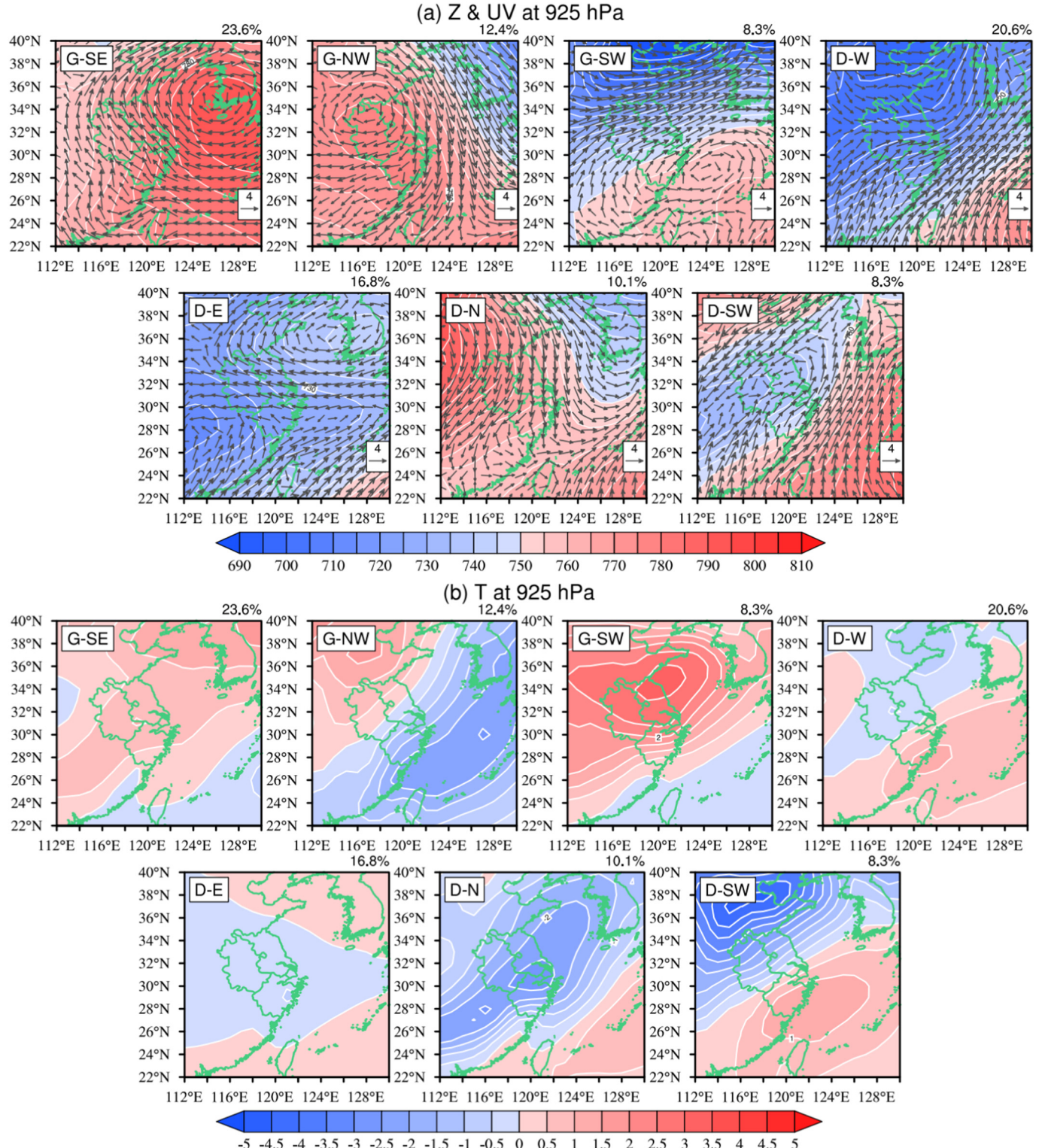


Fig. 3. (a) The structures of geopotential height (white contour and shade, unit: gpm) and wind vectors (black arrow) at 925 hPa for each weather patterns in AMJ. Values at right top indicate the frequencies of the occurrences. (b) Same as (a), but for mean temperature anomalies ($^{\circ}$ C) relative to the previous day.

Shanghai. The predominant weather in Shanghai is more variant, and exhibits rapid evolutions. As a result, it is important to elucidate what weather pattern conductive to high O₃ occurrence during AMJ in Shanghai. In this section, the T-PCA method is used for aggregation on the atmospheric circulations to obtain the predominant weather patterns affecting Shanghai during this period. As showed in Fig. 3a, seven major weather types explained by 88.9% of the total variance are identified according to the structure of the geopotential height in 925 hPa combined with predominant winds around Shanghai, named as G-SE, G-NW, G-SW, D-W, D-E, D-N and D-SW respectively.

Before the onset of summer monsoon, the synoptic at mid-latitude in north hemisphere evolutes by the alternative passage of trough and ridge in the troposphere, leading to the high and low pressures at low level respectively. In Fig. 3a, three members (G-SE, G-NW and G-SW) are obviously related to high pressure (HP) system, that accounts for 45%. In which, the G-SE presents the highest occurrence of 23.6%. The corresponding atmospheric circulation at 925 hPa is described as a large-scale high pressure stably occupying on the ocean with the center at South Korea. Shanghai is located at the eastern bottom of the high pressure, prevailed by southeaster winds in the low troposphere. The warmer air mass from the ocean elevates the temperature at Shanghai by about 0.5–1 °C (Fig. 3b). The atmospheric circulation of G-NW (account for 12.4%) is similar as that of G-SE, but presents a weaker continent high pressure taking over eastern China, usually after a cold front passage. In front of the high pressure, Shanghai is dominated by norther winds from the cold front, consequently, the clear drop of temperature of about 1–1.5 °C is observed around Shanghai in Fig. 3b. The G-SW presents the occurrence of 8.3% appeared mainly in late spring. The atmospheric circulation is different from G-SE and G-NW. The isoheight at 925 hPa is very flat in the north of Shanghai, indicating weak synoptic constrain. Shanghai is located very closely to the center of a small-scale high pressure on the ocean, leading to stagnant weather with weak southwesterlies and over 2 °C temperature risen.

In addition to high pressure related weather patterns, there are other four members associated with low pressure (LP) system. In which, the D-W has the highest occurrence of 20.6%. The strong southwester flows march northwards up to 32°N, and make convergence with the westerlies from the bottom of a cyclone around Shanghai. This type of synoptic provides excellent dynamical conditions for the occurrence of precipitation around Shanghai. The atmospheric circulation in D-E matches very well with a typical invert trough. Shanghai is located at the northern edge of the trough, usually accompanied by cloudy weather and predominant easterlies. The atmospheric circulation in D-N clearly presents a cold trough rapidly passing over eastern China to eastwards, leading to significant cold advection from northern China. Shanghai is dominated by strong norther winds accompanied by over 3 °C temperature dropping. The D-SW mainly occurs in early June with the least occurrence of 8.3%. It presents the typical atmospheric circulation of the quasi-stationary front, called MeiYu affecting YRD region. The rain belt usually persists around the 32°N zone from middle June to early July due to the evenly matched conflicts between warm and cold air mass. As a result, Shanghai experiences the continuous rainy weather, lacking of sunny days for about one month. It was explained for the decline of O₃ from May to June in Shanghai by previous studies (Gao et al., 2017).

3.3. O₃ levels under different weather patterns

In order to understand which weather pattern described in Section 3.2 favorable for high O₃ occurrence during AMJ in Shanghai, the box-plot of daily MDA8 O₃ concentrations during 2010 to 2019 observed at DT and XJH for each weather pattern are compared in Fig. 4. The daily MDA8 O₃ concentrations present similar variations with different weather patterns at the remote site DT and the urban site XJH. As is expected, the MDA8 O₃ concentration under HP related weathers are greater than those in LP related synoptics. In general, the mean

MDA8 O₃ concentrations under LP related weathers range from 60 to 65 ppbv at DT and 40–50 ppbv at XJH respectively, while rise to 70–85 ppbv at DT and 50–65 ppbv at XJH under HP related weathers. The highest MDA8 O₃ concentrations are observed under the weather pattern of G-SW, with over 83 ppbv at DT and 65 ppbv at XJH respectively, presenting significant enhancement of about 20 ppbv relative to other two HP related weathers (G-NW and G-SE). It is suggested that G-SW provides the most favorable conditions of meteorology for O₃ production and accumulation in Shanghai during AMJ period. Whereas in terms of the 4 LP related weathers, the MDA8 O₃ concentrations are more comparable, ranging from 60 to 65 ppbv at DT, and 45–50 ppbv at XJH, indicating the similar meteorological condition with respect to O₃ production.

As mentioned in Section 3.1, both mean daily and MDA8 O₃ concentrations present the highest levels in May during AMJ. The frequency of each weather pattern occurred during AMJ from 2010 to 2019 are calculated and compared to elucidate their potential influences on O₃ level. The HP related weathers (G-SE, G-SW and G-NW) account for 49.2% in May, which is comparable to that in April of 51.3% and significantly higher than the 15.3% occurrence in June. In addition, the G-SW weather with the greatest O₃ concentration accounts for 10.7% in May, which is higher than that in April (9%) and June (3.8%). It is noting that the meteorology in May presents higher temperature than April, and less precipitation compared with June. For example, the mean temperature in May averaged between 2010 and 2019 is 21.6 °C and 19.3 °C at XJH and DT respectively, about 5 °C higher than those in April. The mean precipitation in May during the past ten years is 75 mm and 50 mm observed at XJH and DT respectively, much less than those of 250 mm and 125 mm in June due to the Meiyu influence. As a result, the meteorology in May provides more favorable conditions for O₃ productions relative to April and June.

O₃ is mainly formed in daytime by photochemical reactions, while consumed at night when lacking of sunlight. The daytime O₃ variability could be regarded as the indicator to compare the effects of different meteorology on O₃ production and accumulation supposing the same emissions of its precursors. The mean diurnal variation of O₃ concentrations observed at DT and XJH are presented in Fig. 5 for each weather types. The O₃ concentrations enhance from 7:00 and peak around 14:00, which has been documented by Tang et al. (2008) as the “O₃ accumulation period” in Shanghai downtown. It is resulted from the rapid dissociation of NO₂ by strong UV radiation to prompt O₃ production. Considering the very few anthropogenic emissions at DT, the difference of the “O₃ accumulation period” during early morning to mid-afternoon in each weather types is supposed to be attributed to the different effects of meteorological conditions. As showed in Fig. 5a, O₃ presented the largest increasing variability from 8:00 to 14:00 in G-SW at DT, indicating the most favorable meteorological conditions for “O₃ accumulation”. The increasing rate is calculated as 6.5 ppbv/h for G-SW, followed by 4.2 ppbv/h for G-NW. As a result, the daily maximum O₃ concentration in G-SW reaches 87 ppbv, followed by 72 ppbv in G-NW. By contrast, the increasing rates of O₃ concentration under LP related weathers range from 2 to 3 ppbv/h, which are generally lower than those in HP weathers (especially G-SW), suggesting less conductive to O₃ production. This is consistent with the results in Fig. 4, that higher O₃ levels are usually observed under HP related weathers, with the maximum in G-SW. The similar diurnal variations of O₃ concentration in different weather patterns are also observed in XJH (Fig. 5b), with maximum O₃ variability under G-SW and followed by G-NW and G-SE, indicating the distinctive effects of weather patterns on O₃ concentration at both urban and remote sites. As is expected, the daily maximum O₃ concentration at XJH is lower than that at DT under each weather types, especially for HP related weathers. For example, the daily maximum O₃ concentration observed at XJH is 70 ppbv in G-SW, which is 20% lower than that at DT. Under the high NO_x conditions at XJH, the OH radicals are lost by the reaction of NO₂ + OH → HNO₃ (Sillman and Samson, 1995), leading to the decrease in the reactivity and ensuing O₃ productions (Xu et al., 2019).

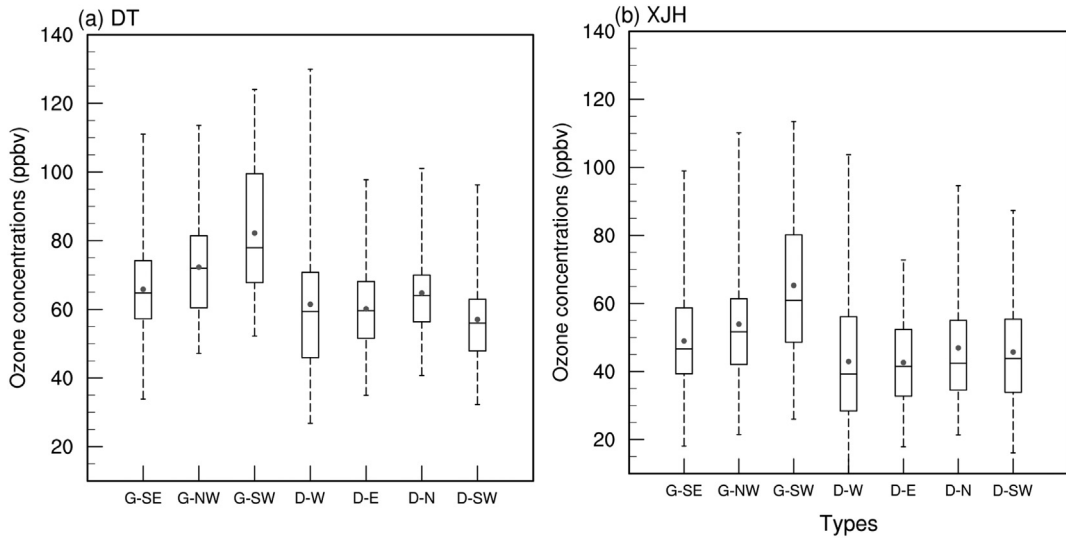


Fig. 4. Box plots of MDA8 O₃ concentrations in AMJ during 2010 to 2019 observed at the (a) DT and (b) XJH for each weather patterns. The bottom, middle and top edges of the box denote the values of the 25th, 50th and 75th percentiles respectively. The dot in the box denotes the mean value.

3.4. Key meteorological factors sensitive to O₃ production in each weather patterns

As is mentioned in Section 3.2, higher O₃ concentrations during AMJ are likely related to HP related weathers, especially under G-SW, the MDA8 O₃ concentrations present the highest level and the most significant increasing rate in daytime. For the purpose to better elucidate what meteorological factors driving the elevated O₃ occurrence in HP related weathers, particularly in G-SW, several weather elements sensitive to O₃ production and accumulation according to the previous studies are examined and compared for each weather types in this section.

The box-plots of mean daily solar radiation, mean daily maximum temperature, mean daily RH and mean wind speed are presented in Fig. 6. Stronger solar radiation and lower RH are expected in HP related weathers. In which, the maximum solar radiation is observed in G-SW of 267 W/m², followed by G-NW and G-SE of about 240 and 212 W/m². In comparison the solar radiations in LP related weathers are much lower with about 124–153 W/m². It is noting that, the solar radiation in G-SW presents most narrow box, indicating much consistent occurrence of sunny weather. This is also well corresponded to the lowest RH below 60% in G-SW in Fig. 6c. In comparable, the solar radiations exhibit broader span box in LP related weathers, also accompanied by higher RH of about 80% (Fig. 6c), suggesting more cloudy and rainy

weather appearance. As showed in Fig. 3a, the LP related weathers are mostly related to strong southwesterlies with plenty of water vapor (D-W, D-SW), or obvious convergence by warm and cold air mass (D-E, D-N), thus providing the excellent conditions for cloud formation or precipitation occurrence. It is noting that the highest daily maximum temperature is also observed under G-SW at 28 °C, indicating the most favorable conditions for O₃ photochemical productions, which agree with the rapidest increasing rate of O₃ accumulation from early morning to mid-afternoon in Fig. 5. While the maximum temperatures under HP related weathers are not completely higher than those under LP related weathers, except G-SW. For example, the maximum temperature under G-SE and G-NW are below 25 °C, which are lower than those under D-W, D-E and D-SW. As a result, lower reactivity is expected for O₃ related chemical reaction cycles under G-SE and G-NW, leading to lower O₃ concentration compared to G-SW in Figs. 4 and 5. In addition, even with higher temperature, O₃ productions are largely inhibited by the lack of solar radiation under LP related weathers. Gu et al. (2020b) also reported the nonlinear relationship between daily maxi-O₃ concentration and maxi-temperature in Shanghai. In terms of horizontal dispersion, the wind speeds range from 2.5 to 3 m/s under different weather types, presenting less variance compared to other three meteorological factors. It is summarized that G-SW is the most favorable weather pattern for O₃ production during AMJ in Shanghai. Both

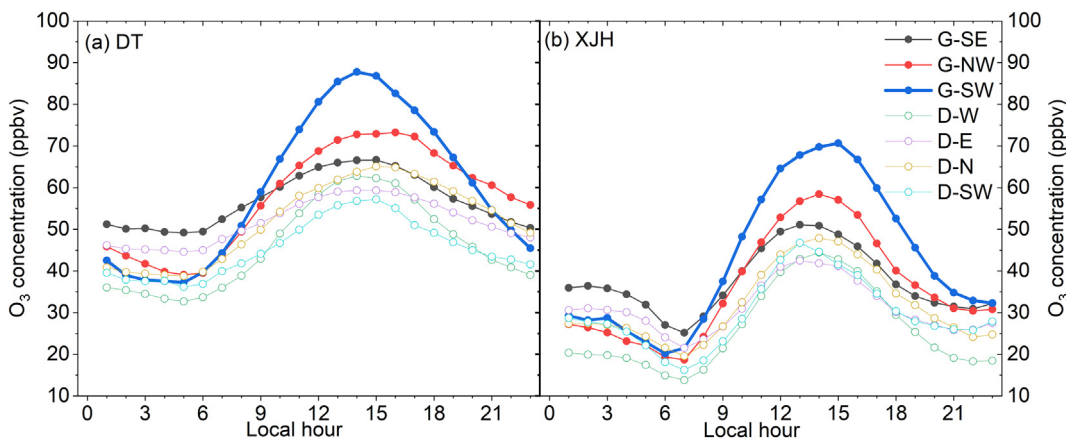


Fig. 5. Diurnal variations of O₃ concentration in AMJ averaged between 2010 and 2019 observed at (a) DT and (b) XJH respectively for each weather patterns.

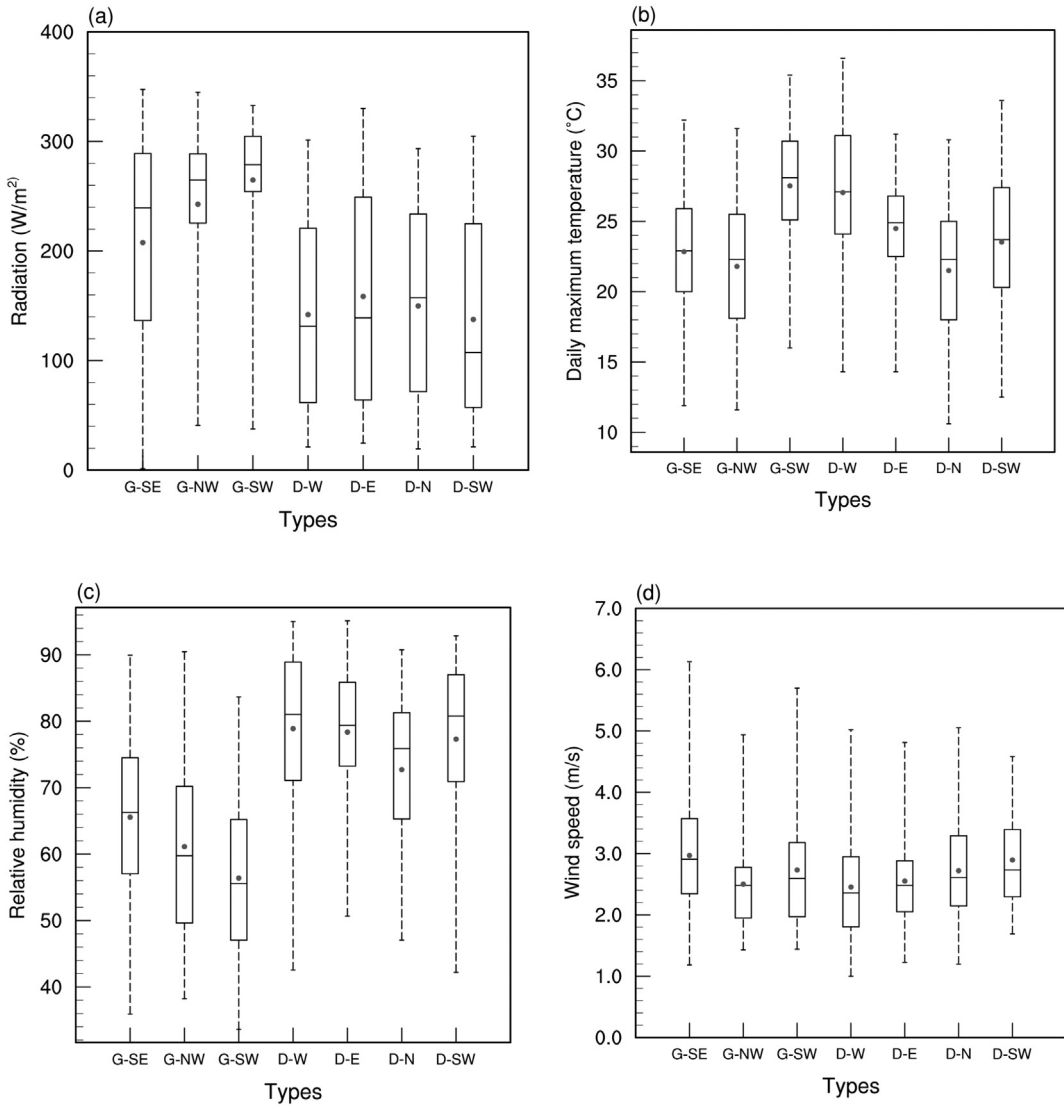


Fig. 6. Box plots of mean daily solar radiation (W/m^2), (b) daily maximum temperature ($^\circ\text{C}$), (c) mean daily RH (%), and (d) mean daily wind speed (m/s) in AMJ from 2010 to 2019 observed at BS observatory in Shanghai. The bottom, middle and top edges of the box denote the values of the 25th, 50th and 75th percentiles respectively. The dot in the box denotes the mean value.

the MDA8 concentration and the O_3 increasing rate in daytime are highest due to the strongest solar radiation and highest daily maximum temperature, providing the best conditions to promote O_3 photochemical formation and accumulation.

Since the G-SW weather is most conductive to high O_3 occurrence, the relationships between daily maximum O_3 concentration and several meteorological factors (including temperature, RH, wind speed and solar radiation) averaged over 3 h around the maximum O_3 occurrence, at the remote site DT are examined by correlation analysis. The maximum O_3 concentration is positively correlated with temperature, and negatively correlated with wind speed, but presenting insignificant correlations with RH and solar radiation. In order to elucidate the synergistic effects of temperature and wind speed on high O_3 occurrence under G-SW weather, the daily maximum O_3 concentrations relative to wind speed and temperature at DT and XJH sites are plotted in Fig. 7. High O_3 concentrations (referred above 100 ppbv) mostly appear when temperature is greater than 30°C , but with the concurrent condition of speed less than 3 m/s. This is more significantly observed at the remote site DT than the urban site XJH perhaps due to the variations of anthropogenic activities. It is noting that there is no appearance of high O_3 concentrations when wind speed beyond 3.5 m/s, even under

the elevated temperature ($>30^\circ\text{C}$) conditions. On the other hand, several high O_3 concentrations are observed under relative low temperature conditions of about 25°C , but constrained by much slow wind speed less than 2 m/s. As a result, wind speeds mostly dominate the capacity of O_3 accumulation. O_3 level is difficult to aggravate under large wind conditions (>3.5 m/s) even with strong O_3 chemical productivities. In addition, O_3 pollution could still be observed under the condition of slow winds (<2 m/s) instead of high temperature.

3.5. Annual variation of MDA8 O_3 concentrations in different weather patterns

Fig. 8 presents the annual variation of MDA8 O_3 concentrations during AMJ from 2010 to 2019 observed at DT and XJH respectively. The MDA8 O_3 concentrations present significant increasing trends for each weather patterns at urban site XJH, ranging from 0.96 to 3.95 ppbv/yr. It is consistent with the documented increasing rate of daily maximum O_3 concentration at XJH by 0.8–1.3 ppbv/yr during 2006 to 2015 (Xu et al., 2019), which was attributed to the significant reduction of NOx emission in recent years. In general, the MDA8 O_3 concentration exhibits higher increasing rates at 2.12–3.95 ppbv/yr under

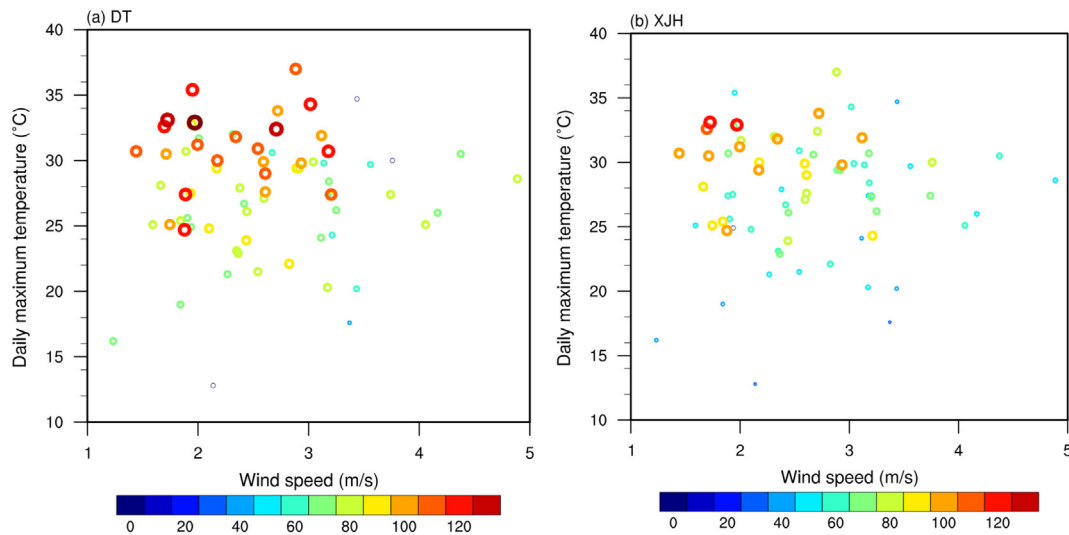


Fig. 7. The relationship of daily maximum O₃ concentrations (ppbv) observed at the rural site (DT) and the urban site (XJH) relative to temperature and wind speed under the G-SW pattern.

HP related weathers than those under LP related weathers of about 0.96–1.82 ppbv/yr. The MDA8 O₃ concentration increases most significantly from 43.7 ppbv in 2010 to 91 ppbv in 2019 under G-SW, presenting the rapidest increasing rate of 3.95 ppbv/yr. These results suggest more and more stronger activities of O₃ productions under HP related weathers, especially G-SW during AMJ in Shanghai downtown by the continuous reduction of NOx emissions. O₃ concentrations measured at the remote site DT are scarcely affected by anthropogenic emissions. As a result, the annual MDA8 O₃ concentrations at DT present insignificant trend, which is consistent with Gao et al. (2017). However, the MDA8 O₃ concentrations observed under G-SW at DT also present substantial increasing rate of 2.42 ppbv/yr from 2010 to 2019. This is puzzling by comparing to the insignificant trend of O₃ variation under other HP and LP related weathers. Tie et al. (2013) suggested that O₃ observed at DT basically reflected on the regional transport from upstream area due to very less anthropogenic emission. Fig. 2a presents the predominant winds at DT under HP related weathers with relatively higher O₃ levels. In which, under G-SE and G-NW, the southeaster and northeaster winds prevail at DT respectively, both carrying the air mass from the ocean to local site. In comparison, predominant southwester winds are observed at DT under G-SW, leading to significant transport from city plumes full of O₃ and its precursors. Such higher O₃ concentration in southwest wind section at DT has also been

reported by Gu et al. (2020a) in spring and summer season. It is expected, the O₃ enhancement resulted from the city plume transport at downwind sites could be greatly strengthened under more sunny weathers (e.g., G-SW) with strong solar radiation and high temperature. In addition to the transport, the long-term variations of meteorological factors under G-SW also need to be checked. The annual variations of G-SW frequency, the T2 and WS, as well as the MDA8 O₃ concentration observed at DT under the G-SW weather during AMJ from 2010 to 2019 are presented in Fig. 9. The frequency of G-SW presents no significant trend (Fig. 9a) during AMJ from 2010 to 2019, while compared to the rapid increasing trend of T2 at the rate of 5 °C per ten years (Fig. 9b) and a notable decreasing trend of WS at the rate of −1.3 m/s per ten years (Fig. 9c) in Shanghai. The mean MDA8 O₃ concentrations observed at DT positively correlated with temperature and negatively correlated with wind speed, with the correlated coefficients of 0.59 and −0.38 respectively both above 95% confidence. It could be speculated that the meteorological elements (especially temperature and wind speed) under G-SW weather pattern tend to be more and more conducive to O₃ production and accumulation during the past ten years. To further quantify their contributions to the increasing O₃ variability at DT, the annual MDA8 O₃ concentrations at DT under the G-SW pattern during AMJ from 2010 to 2019 have been reconstructed (Fig. 9d) by multiple linear regression (MLR) method based on the measurements of T2

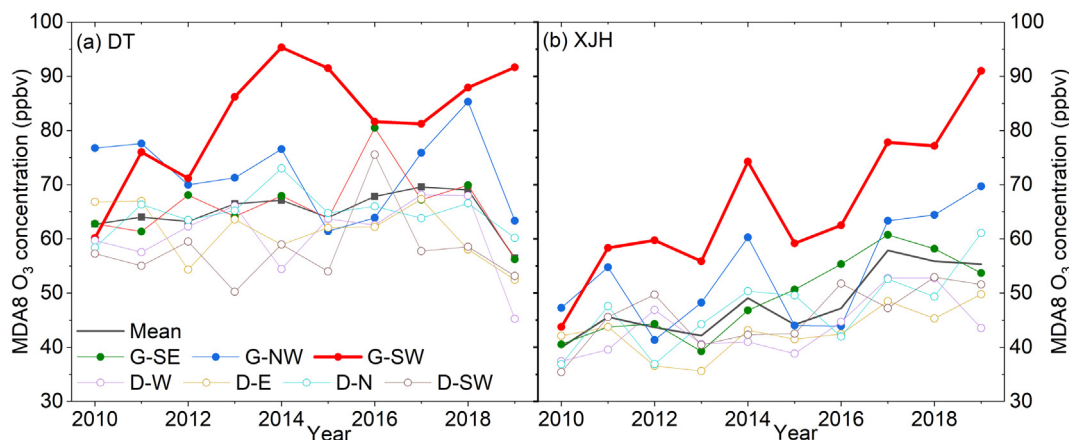


Fig. 8. Annual variation of mean MDA8 O₃ concentrations during AMJ and those under each weather patterns from 2010 to 2019 observed at (a) DT and (b) XJH.

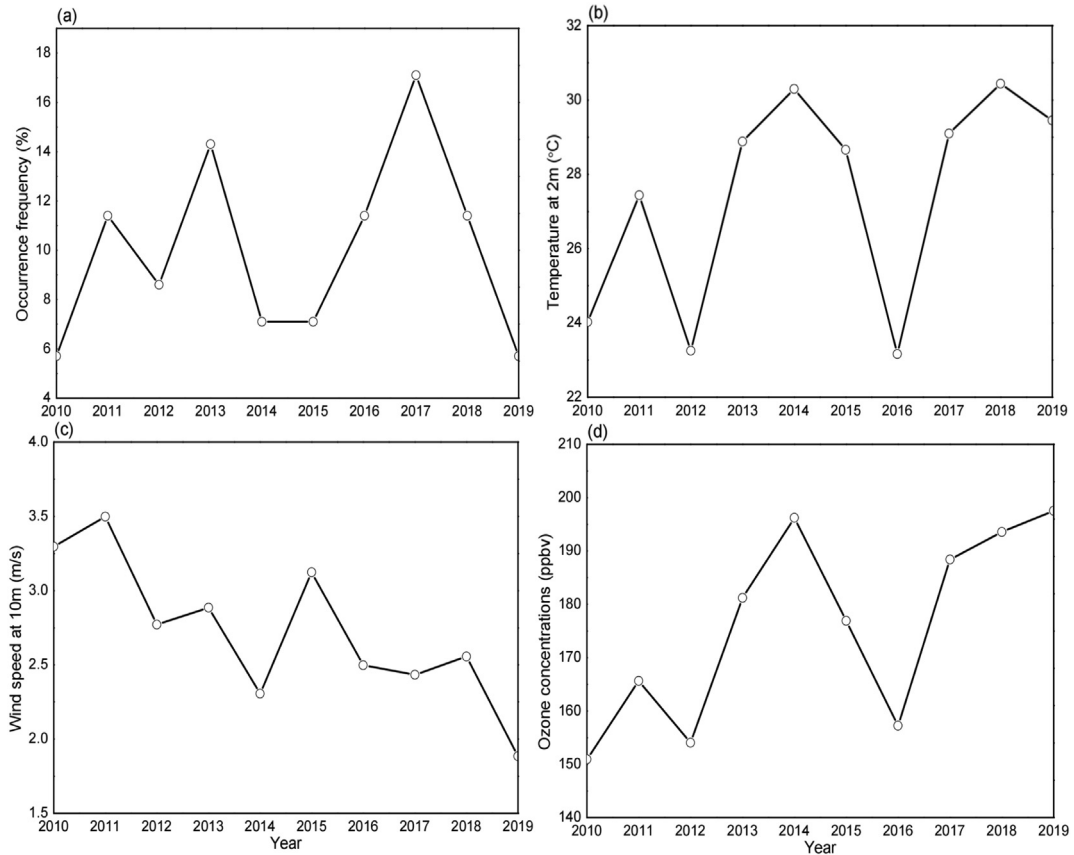


Fig. 9. The annual variations of (a) the frequency of G-SW occurrence (%), (b) 2 m temperature (°C), (c) horizontal wind speed (m/s) observed at BS, and (d) reconstructed MDA8 O₃ concentrations (ppbv) at DT under the G-SW weather pattern during AMJ from 2010 to 2019.

and WS. A notable increasing trend of the reconstructed O₃ data is detected in Fig. 8d, which is highly consistent with the observed 30% enhancement of MDA8 O₃ concentrations from 2010 to 2019 in Fig. 8a, indicating significant contributions from meteorological changes to the substantial O₃ enhancement under G-SW weather during the past ten years. Despite the insignificant change of G-SW occurrence during AMJ from 2010 to 2019, the meteorological conditions under G-SW become more and more favorable for promoting larger O₃ production and accumulation.

3.6. WRF-Chem simulations

The weather pattern of G-SW provides the most favorable condition of meteorology for O₃ production and accumulation. The highest O₃ concentration and the fastest increasing trend under G-SW have also been illustrated in previous sections. It is important to deeply investigate the mechanism of O₃ production in G-SW, then explore the possible effective strategy to mitigate the elevated O₃ occurrence in Shanghai under the weather of G-SW during AMJ. In this section, process analysis is performed for case study by WRF-Chem model to better understand the mechanism of high O₃ formation under G-SW in Shanghai. The different emission reduction strategies are also designed and conducted for effective analysis on peak O₃ alleviations under G-SW.

3.6.1. Model validation

The control simulation is carried out from 20:00 on April 12 to 02:00 on April 16 in 2013, in which, Shanghai was dominated by the typical weather of G-SW on April 15, with clear sky, high temperature, and predominant S-SW winds. The first 48 h simulations are designated as the spin-up. The later 43 h results from 08:00 on April 14 to 02:00 on April 16 are used for process analysis on O₃ budgets. The model performances

are validated by the common metrics (Tie et al., 2009; Xu et al., 2019; Gao et al., 2020) in Table 1, including mean bias (MB), correlation coefficient (R), root mean square error (RMSE) and the index of agreement (IOA) for T2, RH, WS and O₃ concentration simulated by WRF-Chem respectively. The IOA describes the relative difference between the model and observation, ranging from 0 to 1, with 1 indicating perfect agreement. Fig. 10 compares the calculated and observed hourly meteorological factors, including T2, RH and horizontal wind vectors. The WRF-Chem well reproduces the temporal variation of meteorology, with the R both over 0.98 for T2 and RH. The RMSE of simulated T2 and RH are calculated as 1.41 °C and 5.47% respectively, also showing the satisfactory results, indicating that WRF-Chem captures the photolysis condition very well. Particularly, the model exactly reproduces the variations of horizontal wind from northerly on April 14 switching to southwesterly on April 15, suggesting the excellent reflection on the weather evolutions by the model. While the model overestimated the wind speed, with the MB of 1.37 m/s, which should result in excessive dispersion for air pollutants. Fig. 11 presents the simulated and observed hourly O₃ concentrations at DT and XJH respectively. In

Table 1

Model performance metrics including mean bias (MB), correlation coefficient (R), root mean square error (RMSE) and the index of agreement (IOA) for T2, RH, WS and O₃ concentration calculated by WRF-Chem.

	T2 (°C)	RH (%)	WS (m/s)	O ₃ _XJH (ppbv)	O ₃ _DT (ppbv)
MB	-0.04	1.04	1.37	-0.75	-7.05
R	0.98	0.98	0.77	0.87	0.83
RMSE	1.41	5.47	1.68	13.2	13.9
IOA	0.98	0.98	0.59	0.9	0.87

general, the model performs reasonably well on the temporal variations of O₃ concentration at both urban and remote sites, including the clear O₃ diurnal cycles, and the significant enhancement of O₃ on April 15 under the synoptic of G-SW. The magnitudes of calculated O₃ agree well with the observations, with the low RMSE of 13.9 and 13.2 ppbv at DT and XJH respectively, indicating the reasonable emission inventory used in the simulation. However, some discrepancies between the simulations and the observations are also obvious. The model underestimates the maximum O₃ concentration on April 15 by about 30–40 ppbv at both DT and XJH sites. It is likely attributed to the overestimation on the wind speed by WRF-Chem, leading to excessive O₃ dispersions (Xu et al., 2019). In addition, the VOCs species with the high reactivity, e.g., aromatics and isoprene still remain considerable uncertainty in current emissions, which play the important role in the simulation of O₃ production and need to be improved in the future (Tie et al., 2013). In general, the model performs well for both meteorology and O₃ level in the control experiment with the satisfactory IOA of 0.98 for T2 and RH, 0.59 for WS and 0.87–0.9 for O₃, compared to similar studies by Tie et al. (2009) and Xu et al. (2019), providing excellent capacity for further process analysis on O₃ budgets, and sensitive experiments for peak O₃ alleviation.

3.6.2. Process analysis on high O₃ production

As is described in the previous sections, high O₃ level occurred under G-SW is likely attributed to the substantial photochemical production due to strong solar radiation and high temperature. Fig. 12 compared the O₃ tendencies from chemical production, advection and vertical diffusion respectively at urban site XJH. In daytime, surface O₃ is mainly produced by photochemical reactions of its precursors after sunrise, then usually lifted to higher level by turbulence mixing under sunny weathers. At night, the photochemical productions of O₃ cease, O₃ is mainly consumed by titration of NO at urban area, yielding the O₃

gradient between suburb and urban. This could result in O₃ advection from suburb to urban by horizontal winds (Geng et al., 2008). Such budgets of O₃ production and consumption from different process are reasonably reproduced in Fig. 12. For example, the tendencies from chemistry and vertical diffusion are positive and negative respectively in daytime, corresponding to photochemical production and loss from turbulence mixing. While at night, the negative consumption of O₃ is calculated for chemistry, accompanied by positive O₃ advects out of urban center. It is noting that significant O₃ production from chemistry is exhibited from early morning to late afternoon on April 15. The O₃ tendency from chemistry switches from negative to positive at 8:00, then increases dramatically and peaks at 41 ppbv/h at 11:00, due to plenty of NO₂ existed at urban center and elevated solar radiation. This was documented as “O₃ accumulation period” by Tang et al. (2008). Afterward, the chemical tendency declines gradually in the afternoon by reduced NO₂, weaker solar radiation and fresh NO release at late afternoon rush time. In comparison, the tendencies from advection and diffusion in daytime are both negative, with the absolute magnitude below 13 ppbv/h, which is significantly lower compared to that from chemistry. It suggests that photochemistry is the dominant process for high O₃ occurrence under G-SW, which is consistent with the results in previous sections.

3.6.3. Sensitive experiments on high O₃ mitigation

Since photochemistry dominates the local O₃ productions under G-SW in Shanghai urban center, effective strategy of emission reduction should be explored to mitigate possible high O₃ occurrence. According to recent studies by Xu et al. (2019), O₃ formation at XJH was still under VOCs-limited regime after 2016 despite of large NOx reduction combined with less variation of VOCs in recent years. In this section, 4 sensitive experiments are designed to examine the O₃ variations response to different scenario of emission reduction of O₃ precursors

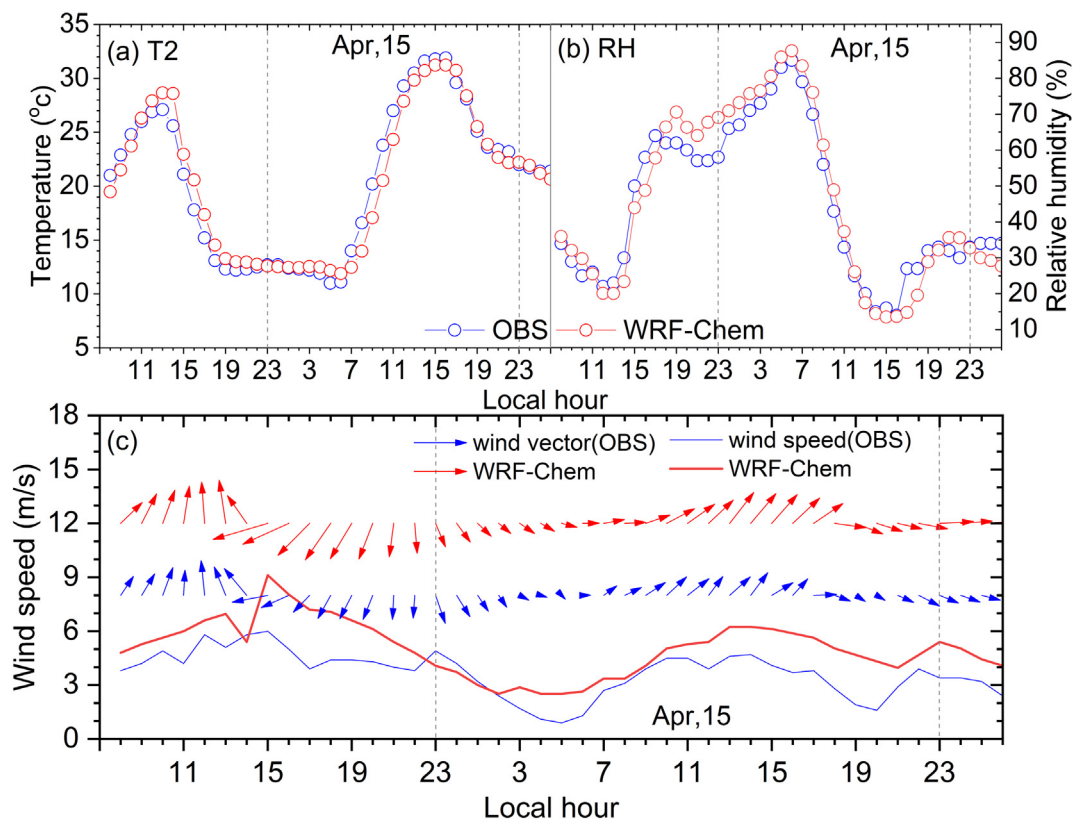


Fig. 10. Comparison of hourly (a) T2, (b) RH and (c) horizontal wind vector and wind speed at BS of WRF-Chem simulations and observations from 08:00 on April 14 to 02:00 on April 16, 2013.

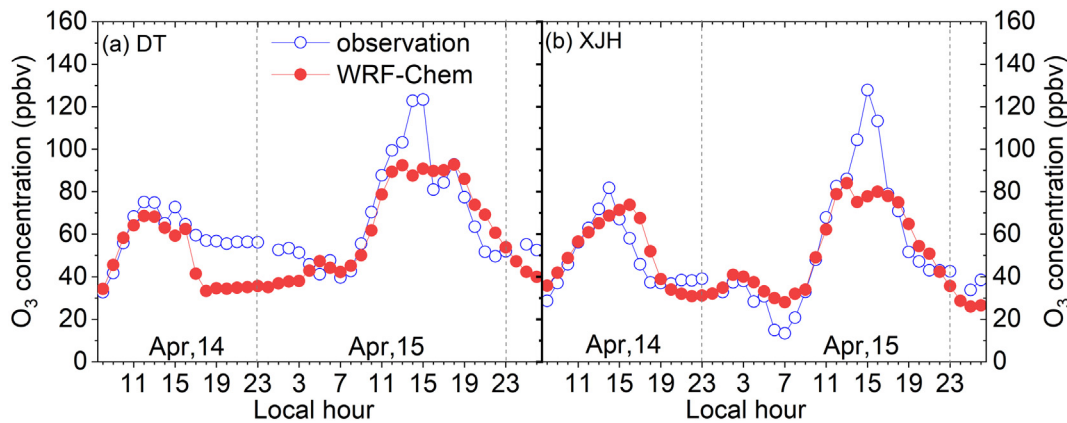


Fig. 11. Comparison of hourly O₃ concentrations at (a) DT and (b) XJH of WRF-Chem simulations and observations from 08:00 on April 14 to 02:00 on April 16, 2013.

over Shanghai: Exp1 and Exp2 are conducted with 30% and 50% reduction of NOx emission respectively, Exp3 and Exp4 with 30% and 50% of VOCs reductions respectively. For the RADM2 gas mechanism used in WRF-Chem, the VOCs are surrogated into 14 species, such as alkane, alkene, aromatics, formaldehyde, etc. In Exp3 and Exp4, all the species of VOCs are reduced consistently. The O₃ tendency from chemistry calculated by Exp1 to Exp4 in daytime on April 15 at XJH is presented in Fig. 13. The O₃ productivity significantly increases from 08:00 to 16:00 response to the NOx reduction. The maximum O₃ tendency arrives at 51 and 60 ppbv/h in Exp1 and Exp2 respectively. This is result from the VOCs-limited regime for O₃ production at XJH. As a result, the peak O₃ concentration rises to 97 and 106 ppbv respectively (Fig. 14), exhibiting 14% and 25% exacerbation than that (85 ppbv) in control test. Xu et al. (2019) suggested that the O₃ concentration at XJH increase by 10–30% response to 50% NOx reduction based on the emission scenario in 2009, which is consistent with the result in Fig. 13. In comparison, the O₃ chemical productivity decreases substantially in daytime response to VOCs reductions in Exp3 and Exp4. For example, with 30% reduction of VOCs emission in Exp3, the O₃ tendency of chemical production drops by 35% in daytime (08:00–16:00), leading to efficient mitigation on both peak O₃ concentration and MDA8 O₃ concentration, which decrease by 17.6% and 14.1% respectively. Moreover, the effect of VOCs reduction on O₃ mitigation is further significant in Exp4, leading to 28.5% decline of peak O₃ concentration (Fig. 14). These results also generally agree with the previous model studies. For example, Geng et al. (2008) suggested that the O₃ concentration at Shanghai urban center increase from 40 ppbv to 100 ppbv response to the enhancement of VOCs concentration from 50 to 150 ppbv by box

model study. Gu et al. (2020b) also reported daily maximum O₃ concentration at XJH decreased by 30% with 15% reduction of VOCs emission under the condition of daily maximum temperature ranging between 28 and 32 °C by WRF-Chem study. In addition, the effects of VOCs reduction on O₃ mitigation are significantly affected by predominant winds. The spatial distribution of the difference of daytime O₃ concentration on 15 April between Exp4 and control test is furtherly analyzed. The decline of O₃ concentrations mainly exists along the transport pathway of city plume. The largest mitigation of O₃ concentration occurs at 50 km downwind of the city, which well agrees with the previous studies. For example, Tie et al. (2013) suggested large O₃ production in city plumes of Shanghai. The O₃ concentrations are significantly enhanced in the city plume extending to 150 km downwind due to doubled VOCs emissions by WRF-Chem studies.

We further extend the sensitive studies to emission control strategy of synergistic reduction on both NOx and VOCs. The other two experiments are conducted by WRF-Chem, referred as Exp5 (50% reduction of VOCs with 30% reduction of NOx emissions) and Exp6 (50% reductions on both VOCs and NOx emissions) respectively. As is expected, NOx reductions lead to clear O₃ enhancement due to the VOCs-limited regime for O₃ chemical production in Shanghai. In Exp5 and Exp6, the additional 30% and 50% reductions of NOx emissions both result in more O₃ productions compared to those in Exp4 with sole VOCs cutdown, which offset the peak O₃ mitigations by 4.8% and 11.6% respectively. As a result, the O₃ concentrations in Exp5 and Exp6

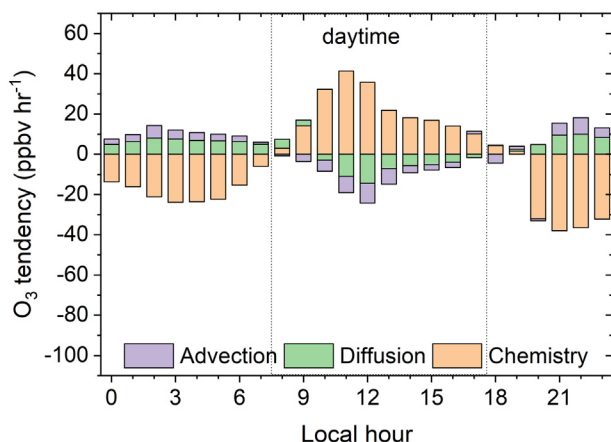


Fig. 12. The hourly O₃ tendency at urban site XJH calculated from chemistry, advection and vertical mixing respectively by WRF-Chem on April 15, 2013.

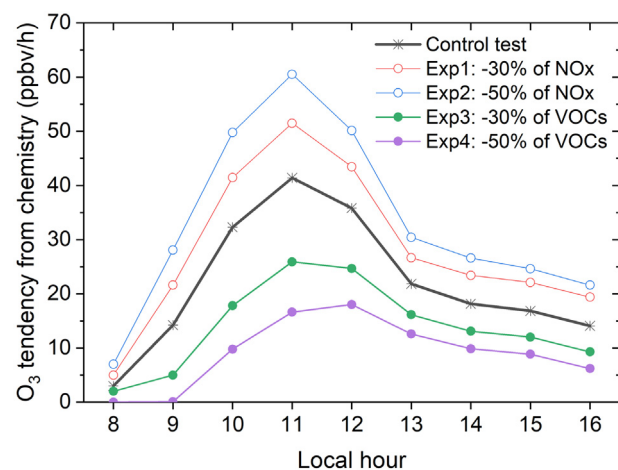


Fig. 13. The hourly O₃ tendency from chemical production in daytime of April 15, 2013 at Shanghai downtown (XJH) in control and sensitive experiments conducted by WRF-Chem model. The 4 sensitive experiments are performed with different scenario of emission reductions: 30% and 50% reduction of NOx in Exp1 and Exp2 respectively, 30% and 50% reduction of VOCs in Exp3 and Exp4 respectively.

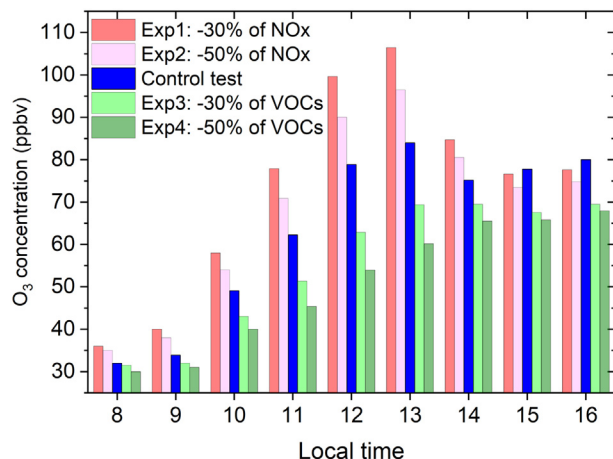


Fig. 14. The hourly O₃ concentration in daytime of April 15, 2013 at Shanghai downtown (XJH) in control and sensitive experiments conducted by WRF-Chem model. The 4 sensitive experiments are performed with different scenario of emission reductions: 30% and 50% reduction of NOx in Exp1 and Exp2 respectively, 30% and 50% reduction of VOCs in Exp3 and Exp4 respectively.

conducted by WRF-Chem with synergistic emission reductions on both NOx and VOCs are enhanced compared to those in Exp4 with individual cutdown of VOCs emissions. These results are consistent with other studies by Tie et al. (2013) and Xu et al. (2019). For example, Tie et al. (2013) suggested that the O₃ chemical production was sensitive to the emission ratios of NOx/VOCs. In Shanghai, the emission ratio of NOx/VOCs was up to 0.4, resulting in strong VOCs-limited regime for O₃ chemical production not only at downtown, but extended to city downwind region. As a result, development of VOCs reduction strategy is more effective and prior for current peak O₃ mitigation under the weather of G-SW in Shanghai, which need be paid more attentions to improve local air quality.

4. Conclusions

More recent studies highlighted the enhanced O₃ level occurred during spring and autumn season in China, but presenting clear distinctions for different cities. In this study, we reveal the greatest O₃ concentrations observed during AMJ in warm seasons in Shanghai based on long-term measurements from 2010 to 2019 at both urban and remote sites. The weather pattern of G-SW is identified by T-PCT method, with the strongest solar radiation and highest temperature favorable for O₃ production and accumulation during AMJ. As a result, the occurrence of the highest O₃ concentration in G-SW is attributed to strong O₃ productivity from chemistry in Shanghai urban center by process analysis of WRF-Chem studies. To mitigate the severe O₃ pollutions in G-SW, emission reduction of VOCs is expected as the effective strategy to decrease peak O₃ concentration in Shanghai downtown by sensitive studies, which is highly suggested to be conducted in Shanghai.

- (1) During warm seasons, the highest O₃ levels are observed in mid-spring to early summer (AMJ) while not in hot summer (Jul) or early autumn (Sep) in Shanghai based on the measurements from 2010 to 2019. The mean MDA8 O₃ concentrations in AMJ are 48.0 ppbv at urban site XJH, and 65.7 ppbv at remote site DT, exhibiting 11% enhancements than the average value in warm seasons.
- (2) Three HP related and four LP related weather patterns dominating Shanghai in AMJ are aggregated by T-PCA method. In which, under the synoptic of G-SW appeared in late May, O₃ exhibits the highest level and the rapidest increasing rate in daytime compared to other weather patterns. The meteorology of G-SW is characterized as the strongest solar radiation and highest

maximum temperature. Consequently, substantial O₃ chemical production is facilitated in daytime, which dominates the high O₃ occurrence in G-SW in Shanghai urban center by model simulations.

- (3) The MDA8 O₃ concentration under G-SW increases significantly from 43.7 ppbv in 2010 to 91 ppbv in 2019, presenting the most increasing rate of 3.95 ppbv/yr at Shanghai downtown compared to other weather patterns. It is indicated that the observed increasing trend of O₃ level during past 10 years in Shanghai is strengthened significantly under the weather pattern of G-SW. As a result, more occurrence and exacerbation of O₃ pollutions under G-SW are expected in Shanghai in the future.
- (4) Sensitive experiments suggest that the photochemical productivity decreases by 35% in daytime (8:00–16:00) under the weather of G-SW, leading to 17.6% mitigation of peak O₃ concentration in Shanghai downtown response to 30% reduction of VOCs emissions. Moreover, the mitigation effect is strengthened by further reduction of VOCs emissions, which is highly suggested for the development of emission control strategy in Shanghai.

CRediT authorship contribution statement

Luyu Chang: Data curation, Visualization. **Fangfang He:** Methodology, Resources, Investigation. **Xuexi Tie:** Methodology, Writing – review & editing. **Jianming Xu:** Investigation, Software, Visualization. **Wei Gao:** Data curation, Investigation.

Declaration of competing interest

The authors declare that they have no known competing financial interests or personal relationships that could have appeared to influence the work reported in this paper.

Acknowledgements

This work is supported by the Ministry of Science and Technology of the People's Republic of China (grant no. 2019YFC0214605), the Science and Technology Commission of Shanghai Municipality (grant no. 19DZ1205003 and 21YF1412400).

References

- Chang, L., Xu, J., Tie, X., Gao, W., 2019. The impact of climate change on the Western Pacific subtropical high and the related ozone pollution in Shanghai, China. *Sci. Rep.* 9, 16998. <https://doi.org/10.1038/s41598-019-53103-7>.
- Copernicus Climate Change Service (C3S), 2017. ERA5: fifth generation of ECMWF atmospheric reanalyses of the global climate. Copernicus Climate Change Service Climate Data Store (CDS) [https://cds.climate.copernicus.eu/cdsapp#!/home](https://cds.climate.copernicus.eu/cdsapp#!/).
- Dang, R., Liao, H., Fu, Y., 2021. Quantifying the anthropogenic and meteorological influences on summertime surface ozone in China over 2012–2017. *Sci. Total Environ.* 754, 142394. <https://doi.org/10.1016/j.scitotenv.2020.142394>.
- Ding, A., Wang, T., 2006. Influence of stratosphere-to-troposphere exchange on the seasonal cycle of surface ozone at Mount Waliguan in western China. *Geophys. Res. Lett.* 33, L03803. <https://doi.org/10.1029/2005GL024760>.
- Ding, A., Fu, C., Yang, X., Sun, J., Zheng, L., Xie, Y., et al., 2013. Ozone and fine particle in the western Yangtze River Delta: an overview of 1 yr data at the SORPES station. *Atmos. Chem. Phys.* 13, 5813–5830.
- Emmons, L.K., Walters, S., Hess, P.G., Lamarque, J.F., Pfister, G.G., Fillmore, D., et al., 2010. Description and evaluation of the Model for Ozone and Related chemical Tracers, version 4 (MOZART-4). *Geosci. Model Dev.* 3, 43–67. <https://doi.org/10.5194/gmd-3-43-2010> 2010.
- Feng, Z., Hu, E., Wang, X., Jiang, L., Liu, X., 2015. Ground-level O₃ pollution and its impacts on food crops in China: a review. *Environ. Pollut.* 199, 42–48.
- Gao, J., Li, Y., Zhu, B., Hu, B., Wang, L., Bao, F., 2020. What have we missed when studying the impact of aerosols on surface ozone via changing photolysis rates? *Atmos. Chem. Phys.* 20, 10831–10844.
- Gao, W., Tie, X., Xu, J., Huang, R., Mao, X., Zhou, G., et al., 2017. Long-term trend of O₃ in a mega city (Shanghai), China: characteristics, causes, and interactions with precursors. *Sci. Total Environ.* 603–604, 425–433.
- Geng, F., Tie, X., Xu, J., Zhou, G., Peng, L., Gao, W., et al., 2008. Characterizations of ozone, NO_x, and VOCs measured in Shanghai, China. *Atmos. Environ.* 42, 6873–6883.

- Goodman, J.E., Prueitt, R.L., Sax, S.N., Pizzurro, D.M., Lynch, H.N., Zu, K., et al., 2015. Ozone exposure and systemic biomarkers: evaluation of evidence for adverse cardiovascular health impacts. *Crit. Rev. Toxicol.* 45, 412–452.
- Grell, G.A., Peckham, S.E., Schmitz, R., McKeen, S.A., Frost, G., Skamarock, W.C., et al., 2005. Fully coupled “online” chemistry within the WRF model. *Atmos. Environ.* 39, 6957–6975.
- Gu, Y., Yan, F., Xu, J., Qu, Y., Gao, W., He, F., et al., 2020a. A measurement and model study on ozone characteristics in marine air at a remote island station and its interaction with urban ozone air quality in Shanghai, China. *Atmos. Chem. Phys.* 20, 14361–14375.
- Gu, Y., Li, K., Xu, J., Liao, H., Zhou, G., 2020b. Observed dependence of surface ozone on increasing temperature in Shanghai, China. *Atmos. Environ.* 221, 117108. <https://doi.org/10.1016/j.atmosenv.2019.11>.
- Guenther, A., Karl, T., Harley, P., Wiedinmyer, C., Palmer, P.I., Geron, C., 2006. Estimates of global terrestrial isoprene emissions using MEGAN (Model of Emissions of Gases and Aerosols from Nature). *Atmos. Chem. Phys.* 6, 3181–3210. <https://doi.org/10.5194/acp-6-3181-2006>.
- Han, H., Liu, J., Shu, L., Wang, T., Yuan, H., 2019. Local and synoptic meteorological influences on daily variability of summertime surface ozone in eastern China. *Atmos. Chem. Phys.* 20, 203–222.
- Hu, J., Li, Y., Zhao, T., Liu, J., Hu, X., Liu, D., et al., 2018. An important mechanism of regional O₃ transport for summer smog over the Yangtze River Delta in eastern China. *Atmos. Chem. Phys.* 18, 16239–16251.
- Huth, R., 1996. An inter comparison of computer-assisted circulation classification methods. *Int. J. Climatol.* 16, 893–922.
- Huth, R., Beck, C., Philipp, A., Demuzere, M., Ustrnul, Z., Cahynova, M., et al., 2008. Classifications of atmospheric circulation patterns. *Annals of the New York Academy of Sciences.* 1146, pp. 105–152.
- Jacob, D.J., Winner, D.A., 2009. Effect of climate change on air quality. *Atmos. Environ.* 43, 51–63.
- Jiang, Y., Zhao, T., Liu, J., Xu, X., Tan, C., Cheng, X., et al., 2015. Why does surface ozone peak before a typhoon landing in southeast China? *Atmos. Chem. Phys.* 15, 13331–13338. <https://doi.org/10.5194/acp-15-13331-2015>.
- Li, M., Zhang, Q., Streets, D.G., He, K.B., Cheng, Y.F., Emmons, L.K., et al., 2014. Mapping Asian anthropogenic emissions of non-methane volatile organic compounds to multiple chemical mechanisms. *Atmos. Chem. Phys.* 14, 5617–5638. <https://doi.org/10.5194/acp-14-5617-2014>.
- Liao, Z., Gao, M., Sun, J., Fan, S., 2017. The impact of synoptic circulation on air quality and pollution-related human health in the Yangtze River Delta region. *Sci. Total Environ.* 607–608, 838–846.
- Lu, X., Hong, J., Zhang, L., Cooper, O.R., Schultz, M.G., Xu, X., et al., 2018. Severe surface ozone pollution in China: a global perspective. *Environ. Sci. Technol. Lett.* 5, 487–494.
- Ma, Z., Xu, J., Quan, W., Zhang, Z., Lin, W., Xu, X., 2016. Significant increase of surface ozone at a rural site, north of eastern China. *Atmos. Chem. Phys.* 16, 3969–3977. <https://doi.org/10.5194/acp-16-3969-2016>.
- Miao, Y.C., Guo, J.P., Liu, S.H., Liu, H., Li, Z.Q., Zhang, W.C., et al., 2017. Classification of summertime synoptic patterns in Beijing and their associations with boundary layer structure affecting aerosol pollution. *Atmos. Chem. Phys.* 17, 3097–3110.
- Ni, R., Lin, J., Yan, Y., Lin, W., 2018. Foreign and domestic contributions to springtime ozone over China. *Atmos. Chem. Phys.* 18, 11447–11469.
- Pu, X., Wang, T., Huang, X., Melas, D., Zanis, P., Papanastasios, D.K., et al., 2017. Enhanced surface ozone during the heat wave of 2013 in Yangtze River Delta region, China. *Sci. Total Environ.* 603–604, 807–816. <https://doi.org/10.1016/j.scitotenv.2017.03.056>.
- Shu, L., Xie, M., Wang, T., Gao, D., Chen, P., Han, Y., et al., 2016. Integrated studies of a regional ozone pollution synthetically affected by subtropical high and typhoon system in the Yangtze River Delta region, China. *Atmos. Chem. Phys.* 16, 15801–15819. <https://doi.org/10.5194/acp-16-15801-2016>.
- Shu, L., Wang, T., Han, H., Xue, M., Chen, P., Li, M., et al., 2020. Summertime ozone pollution in the Yangtze River Delta of eastern China during 2013–2017: synoptic impacts and source apportionment. *Environ. Pollut.* 257, 113631. <https://doi.org/10.1016/j.envpol.2019.113631>.
- Sillman, S., 2003. Photochemical smog: ozone and its precursors. In: Potter, T., Bradley, R.R. (Eds.), *Handbook of Weather, Climate, and Water*. John Wiley & Sons, New York, USA, pp. 227–242.
- Sillman, S., Samson, P., 1995. Impact of temperature on oxidant photochemistry in urban, polluted rural and remote environments. *J. Geophys. Res.* 100, 11497–11508. <https://doi.org/10.1029/94JD02146>.
- Sitch, S., Cox, P.M., Collins, W.J., Huntingford, C., 2007. Indirect radiative forcing of climate change through ozone effects on the land-carbon sink. *Nature.* 448, 791–794.
- Stockwell, W.R., Middleton, P., Chang, J.S., 1990. The second generation regional acid deposition model chemical mechanism for regional air quality modeling. *J. Geophys. Res.* 95, 16343–16367.
- Tang, W., Zhao, C., Geng, F., Peng, L., Zhou, G., Gao, W., et al., 2008. Study of ozone “weekend effect” in Shanghai. *Sci. China Ser. D Earth Sci.* 5, 1354–1360. <https://doi.org/10.1007/s11430-008-0088-2>.
- Tie, X., Brasseur, G., Emmons, L., Horowitz, I., Kinnison, D., 2001. Effects of aerosols on tropospheric oxidants: a global model study. *J. Geophys. Res.* 106, 22931–22964.
- Tie, X., Geng, F., Peng, L., Gao, W., Zhao, C., 2009. Measurement and modeling of O₃ variability in Shanghai, China: application of WRF-Chem model. *Atmos. Environ.* 43, 4289–4302.
- Tie, X., Geng, F., Guenther, A., Cao, J., Greenberg, J., Zhang, R., et al., 2013. Megacity impacts on regional ozone formation: observations and WRF-Chem modeling for the MIRAGE-Shanghai field campaign. *Atmos. Chem. Phys.* 13, 5655–5669. <https://doi.org/10.5194/acp-13-5655-2013>.
- Wang, T., Ding, A., Gao, J., Wu, W., 2006. Strong ozone production in urban plumes from Beijing, China. *Geophys. Res. Lett.* 33, L21806. <https://doi.org/10.1029/2006GL027689>.
- Wang, T., Xue, L., Brimblecombe, P., Lam, Y., Li, L., Zhang, L., 2017. Ozone pollution in China: a review of concentrations, meteorological influences, chemical precursors, and effects. *Sci. Total Environ.* 575, 1582–1596. <https://doi.org/10.1016/j.scitotenv.2016.10.081>.
- Xu, J., Chang, L., Qu, Y., Yan, F., Wang, F., Fu, Q., 2016. The meteorological modulation on PM2.5 interannual oscillation during 2013 to 2015 in Shanghai, China. *Sci. Total Environ.* 572, 1138–1149.
- Xu, J., Tie, X., Gao, W., Lin, Y., Fu, Q., 2019. Measurement and model analyses of the ozone variation during 2006 to 2015 and its response to emission change in megacity Shanghai, China. *Atmos. Chem. Phys.* 19, 9017–9035. <https://doi.org/10.5194/acp-19-9017-2019>.
- Yue, X., Unger, N., 2014. Ozone vegetation damage effects on gross primary productivity in the United States. *Atmos. Chem. Phys.* 14, 9137–9153. <https://doi.org/10.5194/acp-14-9137-2014>.
- Zhang, Y., Mao, H., Ding, A., Zhou, D., Fu, C., 2013. Impact of synoptic weather patterns on spatio-temporal variation in surface O₃ levels in Hong Kong during 1999–2011. *Atmos. Environ.* 73, 41–50. <https://doi.org/10.1016/j.atmosenv.2013.02.047>.
- Zhao, Z., Wang, Y., 2017. Influence of the West Pacific subtropical high on surface ozone daily variability in summertime over eastern China. *Atmos. Environ.* 170, 197–204. <https://doi.org/10.1016/j.atmosenv.2017.09.024>.
- Zheng, Y., Jiang, F., Feng, S., Cai, Z., Shen, Y., Ying, C., et al., 2021. Long-range transport of ozone across the eastern China seas: a case study in coastal cities in southeastern China. *Sci. Total Environ.* 768, 144520. <https://doi.org/10.1016/j.scitotenv.2020.144520>.